PORT SAID ENGINEERING RESEARCH JOURNAL

Faculty of Engineering - Port Said University
Volume 27 No. 4 pp: 102-115

Modeling and Response of Horizontal Axis Wind Turbine Blade Based on Fluid-Structure Interaction

*Eslam Shamso [1, *], Abla El-Megharbel [2], Samar El-Sanabary [3], Rasha M. Soliman [4], Medhat El-Hadek [5]*

[1] *Production Engineering and Mechanical Design Department, Faculty of Engineering, Port-Said University, email: eslam.shamso@eng.psu.edu.eg*

[2] *Production Engineering and Mechanical Design Department, Faculty of Engineering, Port-Said University, email: aelmegharbel@eng.psu.edu.eg*

[3] *Production Engineering and Mechanical Design Department, Faculty of Engineering, Port-Said University, email: samar.abaas@eng.psu.edu.eg*

[4] *Production Engineering and Mechanical Design Department, Faculty of Engineering, Port-Said University, email: rm.soliman@eng.psu.edu.eg*

[5] *Production Engineering and Mechanical Design Department, Faculty of Engineering, Port-Said University, email: melhadek@eng.psu.edu.eg*

** Corresponding author, DOI: 10.21608/PSERJ.2023.239660.1266*

Received 29-9-2023
Revised 19-10-2023
Accepted 22-10-2023

ABSTRACT

Wind energy plays a significant role as a sustainable and renewable energy source. This paper deals with ANSYS to set up computational fluid dynamics (CFD) and structural analysis and then apply for use them to wind turbine (WT) blades. The present paper selected General Electric's (GE) horizontal axis wind turbine (HAWT) for 1.5 MW of renewable energy and focused on using the ANSYS package to calculate the tip velocity, pressure, power coefficient, deflection, flap-wise, and edge-wise deformation values. The simulation analysis considered three independent variables: wind speeds of (7, 10, 12, 15, and 20 m/s), blade position of (90, 180, 270, and 360^0), and Five composite materials of (Carbon-Epoxy, E-Glass, S-Glass, Kevlar, and Technora). The shear stress transport (SST) turbulence was employed. The results show a good agreement between the tip velocity, power coefficient values, and the numerical simulation. The Epoxy E-Glass material exhibits the maximum blade deflection of 1.6363 m, while the Kevlar material has the minimum deflection of 0.41277 m. At a 90^o angle, the Epoxy E-Glass material shows a maximum blade deflection of 1.4918 m, whereas the Kevlar material has a minimum deflection of 0.37381 m at a 270^o angle. These findings highlight the importance of considering wind conditions and their effects on blade performance and structural integrity in wind turbine design and operation.

Keywords: Fluid-Structure Interaction, Composite Materials, ANSYS, Wind Turbine Blade, flap-wise, edge-wise.

1. INTRODUCTION

Wind energy is one of the most used renewable energy sources today to reduce the use of fossil fuels [1,2]. In recent decades, there has been a growing interest among researchers in renewable energy production due to the significant global demand for sustainable power sources as a result, there is an increasing focus on expanding the production capacity of composites, which play a crucial role in developing renewable energy technologies [3,4]. The HAWT length is typically between 17 and 125 m. A HAWT for length of blade 1.5 MW is a wind turbine designed to use electrical energy from wind energy. HAWTs are the most common type of wind turbine used for commercial wind power generation [5–7]. The CFD analysis of a wind turbine (WT) blade is a crucial aspect that requires careful consideration by designers [8–10].

The momentum element blade method (BEM) is the most common method for calculating the aerodynamic load in the wind-power industry [11]. The main reason for most loads in wind turbines is wind speed, which has a random property and can be determined by many factors, such as weather conditions. Therefore, the wind load has an essential role in the design process of a wind turbine [12]. The FSI coupling enables the exchange of information between the fluid and structural domains, leading to a more accurate prediction of the stress distribution and deformation of the blade. The turbulence model SST is a popular CFD model for simulating turbulent flows [11,13,14]. It is a model that combines the benefits of the k-ω and k-models and is especially well-compatible for simulating flows with negative pressure gradients, separation, and reattachment [14]. Many sources, including the work of many researchers, were used to create a satisfying literature survey. Lin Wang et al. [14] used ANSYS FLUENT for CFD. and ANSYS Structure for FEA models to execute FSI on a 1.5 MW. The coupling was carried out on five operational cases, and the flap-wise and edge-wise deflections in each case were compared to other reference analyses. The torque generated by the CFD model was tested against the torque specified in the FAST code. Rajendra Roul et al. [15] studied wind turbine aerodynamics and structural analysis using CFD and FEA. They investigated the influence of different wind velocities and pitch angles on the blade and the importance of considering these factors in blade design. Naji Abdullah Mezaal et al. [16] presented a CFD performance investigation of a HAWT using ANSYS Fluent to confirm the experimental results and validate the power coefficient of the HAWT. Eslam Shamso. et al. [17] presented a study of dynamic simulation in composite HAWT blades using finite element analysis. The study compares the outcomes for various composite materials at different wind velocities and validates the FSI and FEA models with experimental data. This research contributed to understanding the structural behavior of composite blades and their performance in varying wind conditions. Xin Cai et al. [18]. applied the FSI comparing concept in their study and validated the CFD model against a 1.5 MW wind turbine using ANSYS CFX and $k-\omega$ SST turbulent model. Then, applied the BEM method by calculating lift and drag coefficients at 1m intervals. Regarding the finite element model, the blade was modeled with shell elements and composite materials using ANSYS and compared with experimental data. Finally, the stress was simulated through one-way FSI. E. Shamso et al. [19]. conducted to analyze the fatigue life of a HAWT blade subjected to cyclic loads and varying stresses. The analysis focused on applying the Goodman theory to assess the effects of these variable stresses on the blade's fatigue behavior. Michal Lipian et al. [20]. performed investigates using ANSYS to gather data on the structural responses of wind turbines. They obtained surface pressure information from computational fluid dynamics (CFD) results and imported it into the analysis. The new evaluation methods for accurate assessment of the fluid-solid interaction (FSI) process by incorporating the CFD results. E. Shamso et al. [21]. presented the stress analysis of wind turbine blades using CFD and FEA simulations, specifically for HAWT. The study utilizes the software ANSYS for modeling complex shapes and simulating FSI. The CFD model calculates aerodynamic loads, while the FEA model determines structural blade responses.

Previous literature has focused on modeling the influences of different wind speeds specific to the efficiency of HAWT. However, to accurately calculate the stresses and deformations on the turbine blades, it is necessary to conduct additional calculations considering various flap-wise and edge-wise deformations at different positions along the blade. As a result, the present research aims to complement the existing studies by utilizing ANSYS software for CFD analysis and FE analysis calculations. The research methodology's structure is illustrated in Figure 2, which displays a flow graph of the CFD modeling employed in the study.

2. METHODOLOGY

The methodology of this study involved several key steps in conducting the CFD and structural analysis of the HAWT. The following outlines the methodology: Geometry and mesh generation, boundary conditions, solver settings, CFD, simulations, post-processing, and structural analysis.

2.1. Aerodynamic theories

The given model assumes that the airflow is incompressible, flows straight, and has rotational symmetry. It applies the principles of conserving mass and momentum to the annular control volumes surrounding the flow, as illustrated in Figure 1 [11,22].

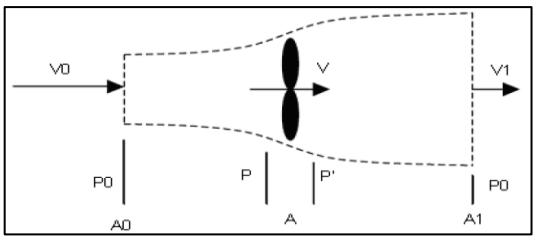

Figure 1: The axial stream tube model [11,22].

Applying mass conservation to the control volume results in the following:

$$V_o A_o = VA = V_1 A_1 = V_i A_i \quad (1)$$

By conserving linear momentum in the axial direction,

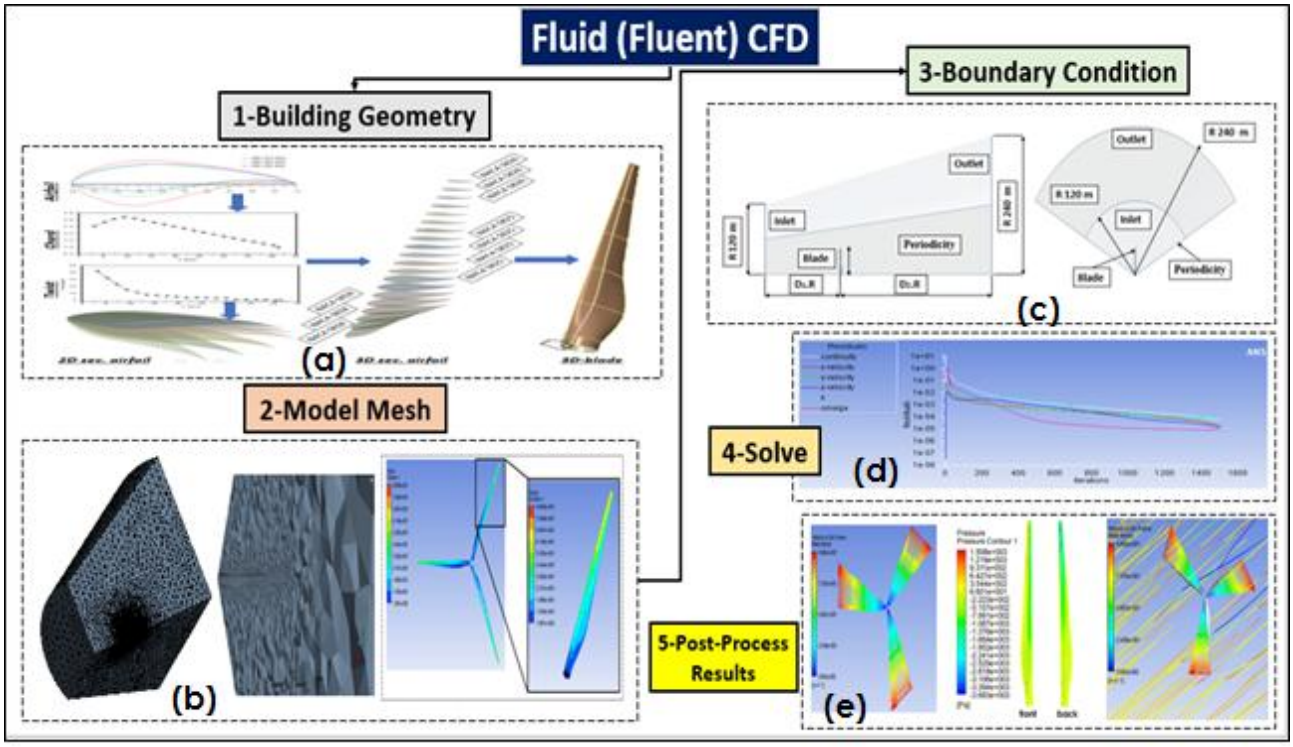

Figure 2: Flow chart of methodology

the thrust force F_T at the rotor disc can be determined within the control volume.

$$F_T = m(V_o - V_1) = \rho AV(V_o - V_1) \tag{2}$$

Where F_T is thrust force, (m) is mass and V is wind velocity, ρ is density and A is area.

The pressure difference across the rotor plane can be obtained by applying Bernoulli's Equation:

$$p - p' = \frac{1}{2}\rho(V_o^2 - V_1^2) \tag{3}$$

The thrust is given as:

$$F_T = \frac{1}{2}A\rho(V_o^2 - V_1^2) \tag{4}$$

The velocity of the flow passing through the rotor can be determined by taking the average of the velocities in the upwind (free stream) and downwind directions:

$$V = \frac{V_o + V_1}{2} \tag{5}$$

The rotor's power:

$$P = \frac{1}{2}m(V_o^2 - V_1^2) = \frac{1}{2}A\rho V(V_o^2 - V_1^2) \tag{6}$$

The power coefficient, C_P, is defined as:

$$C_P = \frac{P}{\frac{1}{2}\rho AV_o^3} \tag{7}$$

The axial interference factor, [a]:

$$V = (1 - a)V_o \tag{8}$$

$$a = \frac{V_o - V}{V_o} \tag{9}$$

The trust expression of Equation (4) becomes:

$$F_T = \frac{1}{2}\rho AV_o^2\ 4a(1 - a) \tag{10}$$

The power extracted by the rotor is:

$$P = \frac{1}{2}\rho AV_o^3\ 4a(1 - a)^2 \tag{11}$$

The expression of C_p becomes:

$$C_P = 4a(1 - a)^2 \tag{12}$$

$$C_{Pmax} = \frac{16}{27} = 0.5926 \tag{13}$$

2.2. Computational fluid dynamics (CFD)

The simulation is established on the continuity and Navier-Stokes equations. This method enhances the efficiency of the simulation. In particular, the conservation of mass equation is utilized in Equation (14) [10]. The mass conservation equation presented is a general equation that can be used for both compressible and incompressible flows. Additionally, another equation can be used to express the conservation of momentum in a reference frame that is not accelerating, as presented in Equation (15). Solving the equations is challenging and often requires approximations or simplifications. Various numerical methods and CFD techniques are commonly used to solve these equations and analyze fluid flow in different applications, including wind turbines [23].

$$\frac{\partial_\rho}{\sigma_t} + \nabla.(\rho\vec{u}) = 0 \tag{14}$$

$$\partial t/\,\partial\,(\rho\vec{u}) + \nabla\cdot(\rho\vec{u}\vec{u}) = -\nabla p + \nabla\cdot(\bar{\bar{\tau}}) + \rho g + F \tag{15}$$

Where $\partial\rho/\partial t$ is the partial derivative of density ρ for time t; ∇ is the del operator (gradient). $\partial t/\,\partial\,(\rho\vec{u})$ is the partial derivative of the momentum $\rho\vec{u}$ for time t, p is the pressure, F represents any external forces acting on the fluid.

Table 1. HAWT 1.5 MW [17,24]**.**

Parameters	Values	units
Power	1.5	MW
NREL section types	S818 -S825-S826	
Rotor radius R_r	41.25	m
Free stream velocity V_w	7,10,12,15, and 20	m/s
Rotational Speed ω	21.21	rpm
Air density	1.225	kg/m^3

2.3. Model of a Wind Turbine Blade

The HAWT length is around 30 m. The CFD analysis of a blade under wind flow is crucial for designers. One of the primary concerns for designers is the CFD analysis of a blade in the wind flow. CFD of a WT blade design is the first step to testing and validating the design. This study selected GE's HAWT for 1.5 MW of renewable energy as a case study [5,8,25]. The necessary data on this turbine is presented in Figure 3 and Table 1 [14,24,26].

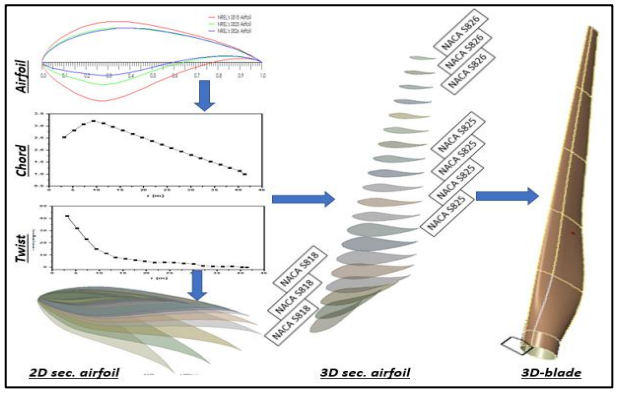

Figure 3: Model HAWT 1.5 MW.

2.4. CFD modelling

The CFD simulation of WT blades are created by ANSYS fluently and is commonly used as a CFD modeling package [10]. The CFD case is used for modeling a 1.5 MW blade wind turbine. This section contains the meshing, boundary conditions, post-processing, and convergence conditions used in the modeling of CFD.

2.4.1. Computational domain and boundary conditions

The computational domain of the model in this study includes the entire blade and a portion of the surrounding air. The blade is discrete into many small elements, and the fluid flow over each element is analyzed using ANSYS Fluent software [10,27,28]. The model's boundary conditions are set to simulate real-world conditions, including the incoming wind velocity, the outlet's pressure, and the blade's rotational motion. It is symmetrical around its center of rotation, and the three-blade design allows for a single blade to be analyzed in a 120º radial stream tube field with rotating surfaces, as shown in Figure 4 [14,17,24,29]. The CFD analysis component of the ANSYS workbench is utilized for this purpose, as shown in Figure 4. The CFD modeling boundary condition (BC) can be set once the blade design modeler, material, element size, and loads have been defined. The main properties of airflow, such as density, pressure, and viscosity, are 1.225 kg/m^3, 101325 Pa, and 1.7894×10^{-5} kg/m, respectively. The analysis results are obtained for essential parameters such as tip velocity, pressure contours, and other aerodynamic characteristics.

Table 2. Mesh independency study

Item	Mesh independency study					
El. size (m)	0.5	0.4	0.3	0.2	0.1	0.08
Rotor torque (KN.m)	156.611	206.346	265.684	362.181	428.924	443.230
No. of Elements	310,177	362,580	453,694	707,741	1,982,295	2,855,058

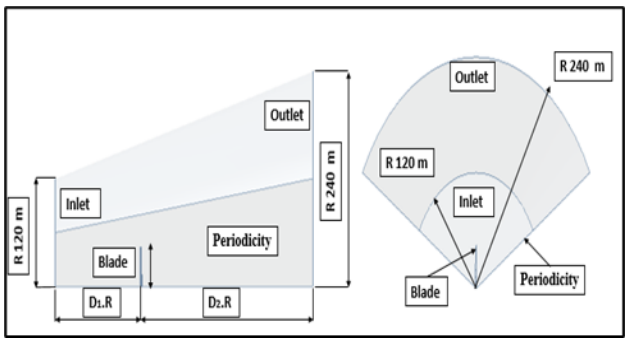

Figure 4: CFD modeling and boundary conditions

2.4.2. CFD mesh

In this study, the default meshes provided by ANSYS CFD are used, and the meshing strategy has been reformed to ensure local control over sizes around different engineering entities. The value of y+ is calculated as the product of the dimensionless wall distance and the friction velocity divided by the kinematic viscosity of the fluid presented in Equation (16). Figure 5 presents the mesh used in the CFD modeling and distribution of blade y+. The value of y+ is used to guide the selection of the appropriate mesh resolution near the walls. It is important to note that the mesh used in this analysis has been optimized to balance accuracy and computational efficiency. The height of the first layer is 4.8×10^{-6}m with a growth rate of 1.35 and 20 inflation layers. A y+ value less than one is recommended for accurate boundary layer modeling, as shown in Figure 5 (c) [10,14].

$$y^{+} = \frac{u_{*}\times y}{\nu} \tag{16}$$

Where y+ is the dimensionless wall distance, u* is the friction velocity, y is the distance from the wall, and ν is the kinematic viscosity of the fluid.

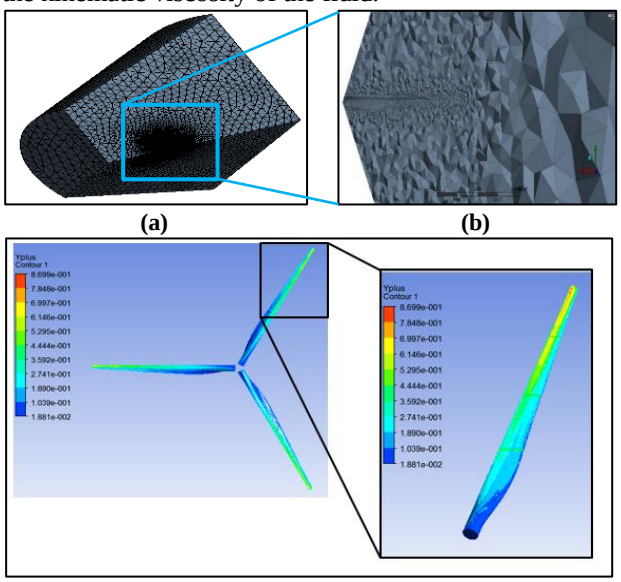

(a) **(b)**

(C)

Figure 5: (a) CFD mesh (b) The inflation in the blade surface. (C) The distribution of blade y+

2.4.3. Mesh study on CFD.

The following element sizes are investigated at blade surfaces: 0.5 m, 0.4 m, 0.3 m, 0.2 m, 0.1 m, and 0.08 m. Figure 6 and Table 2 show the number of elements and the torque. Figure 6 and Table 2 show that the torque converges at an element size of 0.1 m. Further refinement of the element size significantly increases the computational time; an element size of 0.1 m is estimated in this study.

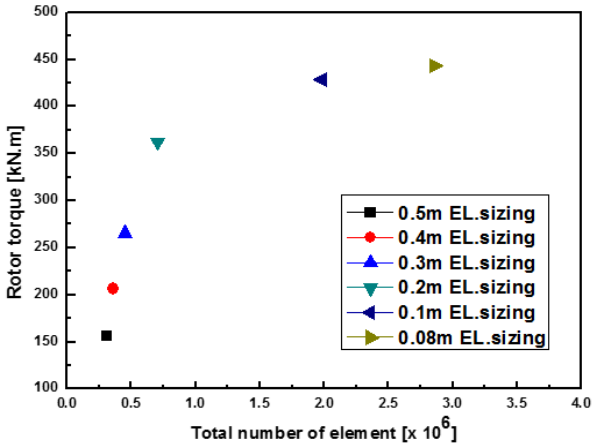

Figure 6: Mesh independency study

2.4.4. Turbulence model and solution methods

The kω - (SST) model was used in this study [10]. This model offers the advantage of transitioning from kω-form disorder, which is appropriate for distant field flow simulation, to kω-form disturbance, which is suited for boundary layer modeling. This model has been widely used in blade research and has produced positive results presented in Equation (17,18) [14].

$$\partial/\partial t\ (\rho k) + \partial/\partial xi\ (\rho k u_i) = \partial/\partial xj\ (\Gamma k\ \partial k/\partial_{xj}) + G_k - Y_k + S_k \tag{17}$$

$$\partial/\partial t\ (\rho\ \omega) + \partial/\partial xi\ (\rho\ \omega u_{i)} = \partial/\partial xj\ (\Gamma\omega\ \partial\omega/\ \partial_{xj}) + G_\omega - Y_\omega + D_\omega + S_\omega \tag{18}$$

Where: G_k represents the generation of turbulence kinetic energy due to mean velocity gradients.

2.4.5. CFD simulation

A steady-state CFD of simulation using a pressure-based approach was conducted in this study, with the turbulence model being (SST). Pressure-velocity coupling was employed in the solution methods. The momentum equation was evaluated using a second-order upwind algorithm, while a first-order upwind was used for turbulent kinetic energy and specific rate. The residual is one of the most widely used methods for determining CFD solution convergence. Convergence was completed by checking residuals up to 1500 iterations, as shown in Figure 7.

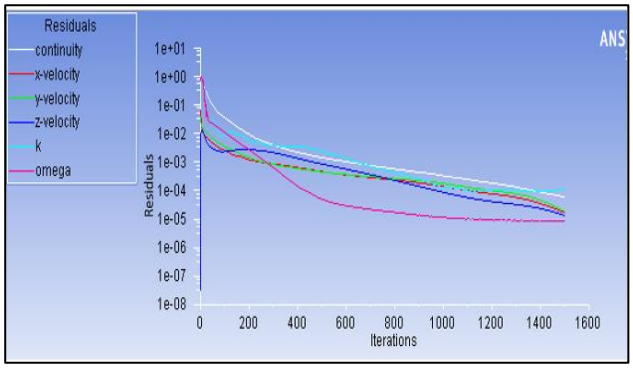

Figure 7: Residuals study in ANSYS fluent

3. FE MODELLING AND MATERIAL PROPERTIES

ANSYS Workbench is a general FEA software package [30,31]. Composite materials are essential in manufacturing wind turbines, horizontal or vertical, due to their lightweight and efficiency in obtaining the best value for energy. Wind turbine composites include Fiber Glass, S-Glass, and Carbon Fiber [17]. In this study, the CFD analysis in the ANSYS workbench rotor blades are made of the most common composite materials: Fiber Glass and Carbon-Epoxy. Table 3 shows the composite materials used in reference [24,32].

Table 3. Material properties of composite materials [17,24,32].

Material	*Epoxy-S-Glass*	*Epoxy-E-Glass*	*Epoxy-Carbon*	*Kevlar*	*Technora*
E (GPa)	50	45	121	179	70
υ	0.3	0.3	0.27	0.3	0.3
ρ (kg/m^3)	2000	2000	1490	1470	1390

3.1. Boundary conditions for FSI

To study the performance of the WT during regular operation, a one-way coupling model is required as the data are exchanged between the CFD and the FE models, and each one affects the results of the other. In the FE analysis, the structural module of the blade is constructed, considering fixed support from the blade's root. In addition to the aerodynamic loads, other essential forces, such as gravitational and centrifugal forces, are also considered. These forces, along with the aerodynamic loads, influence the performance of the wind turbine during regular operation. The pressure distribution obtained from the CFD analysis is imported into the FE model, as shown in Figure 8, to perform the structural analysis. Gravitational and centrifugal forces, in addition to aerodynamic loads, influence wind turbine performance during regular operation. As illustrated in Figure 8, these forces are applied to the FE model. Both loads affect the flap-wise and edge-wise deflection at the 90^o, 180^o, 270^o, and 360^o positions.

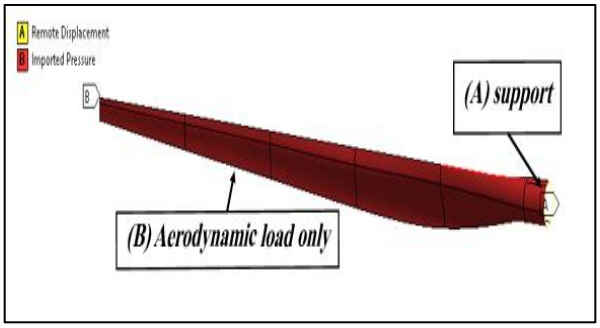

(a) Aerodynamics load only

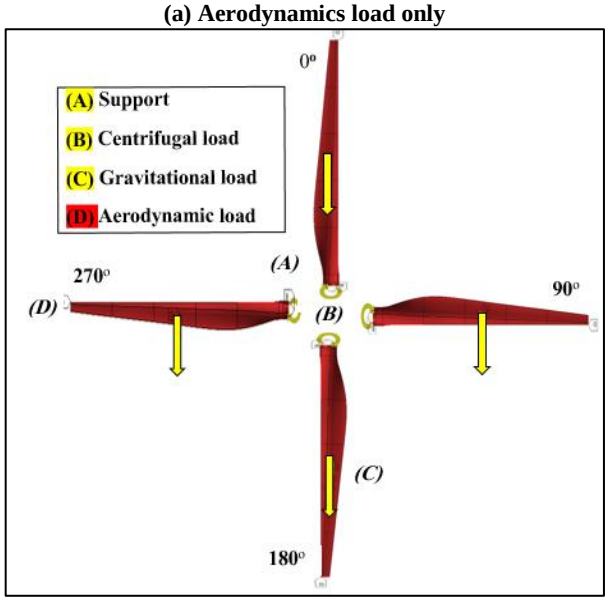

(b) Centrifugal and (c) Gravitational loads

Figure 8: Applied loads (a) aerodynamics, (b) centrifugal, and (c) gravitational loads at each blade position

4. RESULTS AND DISCUSSIONS

4.1. CFD results

This section presents wind turbine blades' tip velocity, power coefficient, and pressure distribution. The velocity of the WT blades refers to the speed at which the air moves past the blades. The power coefficient measures the wind turbine's efficiency in converting the wind's kinetic energy into mechanical power. It is calculated by dividing the actual power output of the turbine by the maximum possible power that could be extracted from the wind. The pressure on the WT blades is the force exerted by the wind on the surface of the blades. This pressure difference between the leading and trailing edges of the blades generates lift, which is the main mechanism responsible for the rotation of the rotor. The design of the blades plays a crucial role in optimizing the pressure distribution and maximizing power generation.

4.1.1. Verification for blade velocity

The local blade velocity increases with radius, with the velocity at the tip being the maximum value. This pattern can be observed in the CFD results and is consistent with the theoretical calculation of the maximum tip velocity, where ω is the angular velocity, and R_r is the blade's radius. The theoretical calculation validated the maximum blade velocity obtained from the CFD analysis. The analytical calculations showed a tip velocity of 96.015 m/s, whereas the CFD analysis indicated a slightly higher velocity of 98.05 m/s, with a difference of approximately 2.07%. The maximum velocity at the blade's tip is higher than at the root, consistent with the expected velocity distribution for a wind turbine blade, as shown in Figure 9.

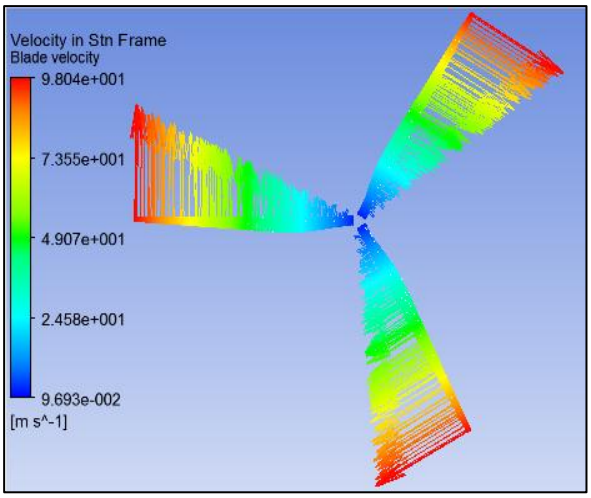

Figure 9: Wind velocity at the tip

4.1.2. Verification for power coefficient

The results show the outcome of combining ANSYS CFD numerical data for power coefficient with analytical computations in Equation (12). These CFD results were compared to the calculated analysis and experimental data obtained from the 1.5 MW report [16]. The results match well, as shown in Table 4.

Table 4. Comparison of results between ANSYS and theoretical

Parameter	Power coefficient (C_p)		(%) Error
	GE 1.5-xle Turbine [16]	**ANSYS CFD**	
Power coefficient (C_p)	0.26	0.28	7.6%

4.1.3. Wind velocity streamline

Visualising the flow around the wind turbine with streamlines can provide insights into the wake behaviour and the turbine's impact on the fluid flow. As shown in Figure 10, the streamlines can be used to visualize the flow behavior before and after the turbine. In the inlet of the domain, the incoming wind velocity is. As the fluid flows over the turbine blade, it experiences a drop in velocity due to the aerodynamic load acting on the blade. The wake behavior is a critical factor in wind turbine design, as it can impact the performance of downstream turbines in a wind farm. By analyzing the wake show of a wind turbine, designers can optimize the position of turbines in a wind farm.

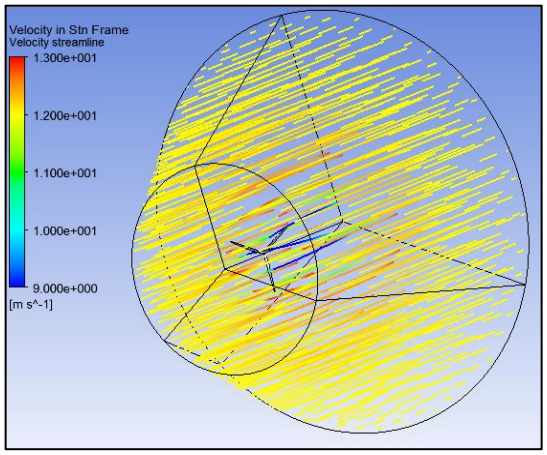

(a)

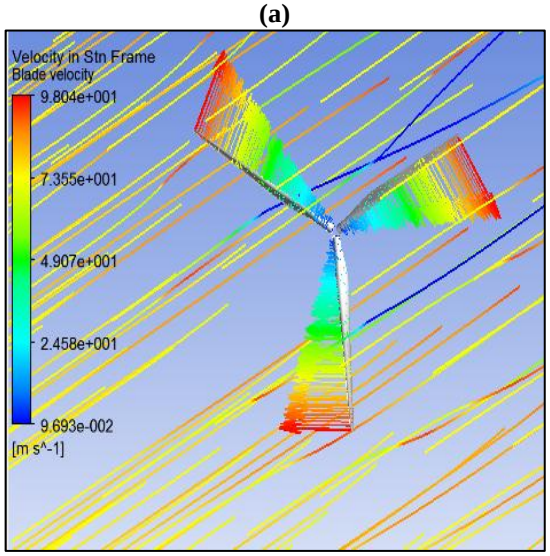

(b)

Figure 10: (a) Velocity streamline (b) blade velocity in ANSYS fluent

4.1.4. Pressure distribution

The pressure distribution over the blade's surface is not uniform, as shown in Figure 11. The pressure on the front surface of the blade is higher than the pressure on the back surface, which creates a pressure difference that generates lift and contributes to the aerodynamic performance of the blade at a similar time. This pressure difference creates a drag force that acts against the direction of motion of the blade and can reduce its efficiency. So, the pressure difference between the back and front surfaces is shown in Figure 11.

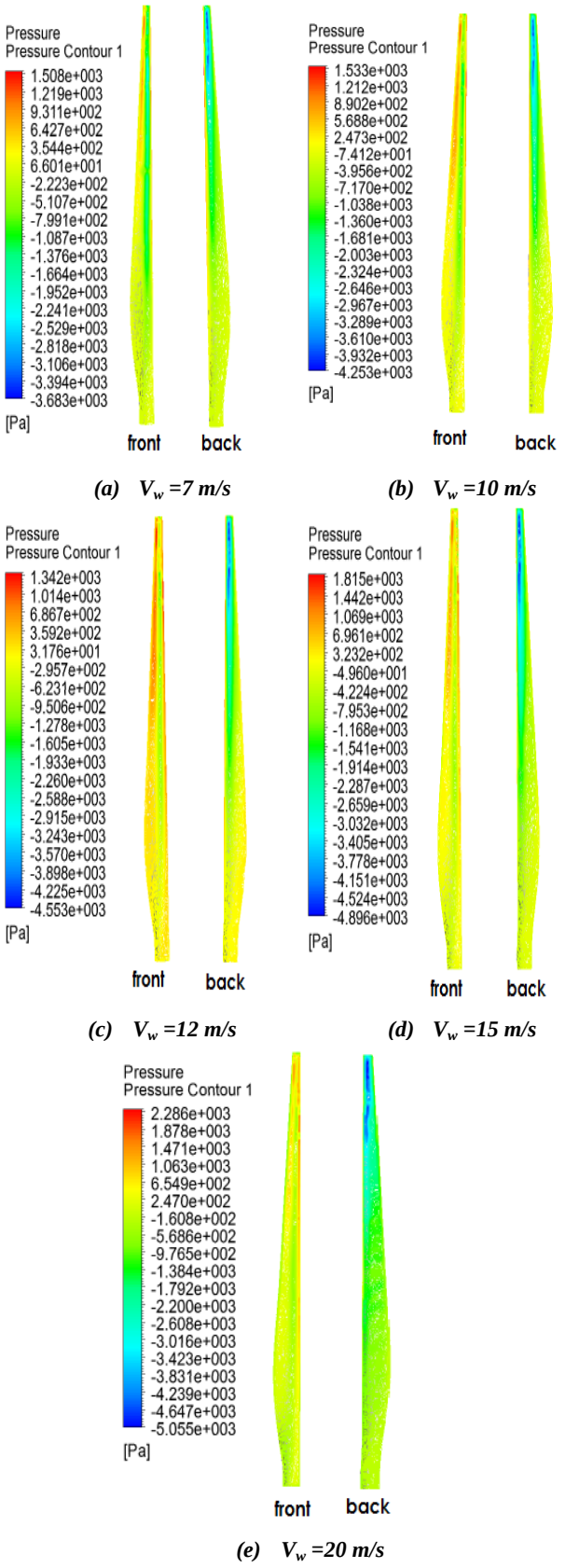

Figure 11: Pressure contours at different velocities (a) 7, (b) 10, (c) 12. (d) 15, and (e) 20 m/s

4.2. Structural results

4.2.1. Deformation for aerodynamic load only

Figure 12 shows the deformation, flap-wise deflection, and edge-wise deflection of five composite materials under aerodynamic load only and wind velocities varying. The deformation of all composite materials shows a significant increase over the range of wind velocities. At a wind velocity of 20 m/s, the maximum deformation values for the different materials are calculated as follows: 0.61 m, 1.63 m, 1.47 m, 0.41 m, and 1.05 m. Similarly, the flap-wise deflection values at 20 m/s are 0.59 m, 1.59 m, 1.44 m, 0.40 m, and 1.03 m for the respective materials. The edge-wise deflection values at 20 m/s are 0.12 m, 0.34 m, 0.30 m, 0.086 m, and 0.22 m. Table 5 compares the ANSYS results for the deformation, flap-wise deflection, and edge-wise deflection at wind velocities and includes the corresponding analysis results. The analysis values are fully shown in Figure 13, obtained through one-way coupling of the FSI model for HAWT. These findings demonstrate the effects of wind velocities on the deflection of composite materials in HAWTs. The ANSYS analysis and FSI model results provide valuable insights into WT blades structural behavior and performance under varying wind conditions. In this section, the paper presents the results of the structural analysis conducted on the blade. The focus is evaluating the stresses and deformations at various blade positions under different loading conditions.

Table 5. Deformation, Flap-Wise, and Edge-wise Deflection for aerodynamic load

	Aerodynamic load - (**Epoxy-Carbon**)		
Velocity (m/s)	Deflection (m)	Flap-wise Deflection (m)	Edge-wise deflection (m)
7	0.20781	0.20411	0.03908
10	0.35269	0.3454	0.071391
12	0.43804	0.42857	0.090672
15	0.54286	0.53073	0.11416
20	0.61038	0.59691	0.12754
	Aerodynamic load - (**Epoxy-E Glass**)		
Velocity (m/s)	Deflection (m)	Flap-Wise Deflection (m)	Edge-wise Deflection (m)
7	0.55809	0.54814	0.10504
10	0.94694	0.9273	0.19159
12	1.1755	1.1499	0.24304
15	1.4559	1.423	0.30555
20	1.6363	1.5997	0.34114
	Aerodynamic load - (**Epoxy-S Glass**)		
Velocity (m/s)	Deflection (m)	Flap-Wise Deflection (m)	Edge-wise Deflection (m)
7	0.50239	0.49344	0.094545
10	0.85251	0.83484	0.1725

12	1.0583	1.0353	0.21886
15	1.311	1.2815	0.27524
20	1.4734	1.4405	0.30732
	Aerodynamic load - (**Kevlar**)		
Velocity (m/s)	Deformation (m)	Flap-Wise Deflection (m)	Edge-wise Deflection (m)
7	0.14052	0.13802	0.026424
10	0.23853	0.2336	0.048281
12	0.29619	0.28978	0.061318
15	0.36701	0.3588	0.077206
20	0.41277	0.40366	0.086278
	Aerodynamic load - (**Technora**)		
Velocity (m/s)	Deformation (m)	Flap-Wise Deflection (m)	Edge-wise Deflection (m)
7	0.35905	0.35266	0.067551
10	0.60938	0.59678	0.12333
12	0.75658	0.7402	0.15654
15	0.93749	0.91649	0.19699
20	1.0539	1.0306	0.22003

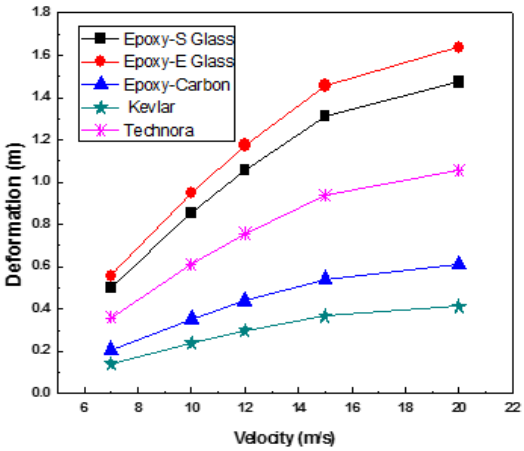

(a)

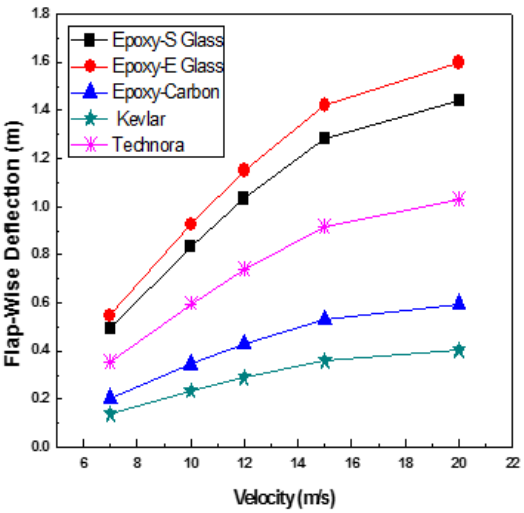

(b)

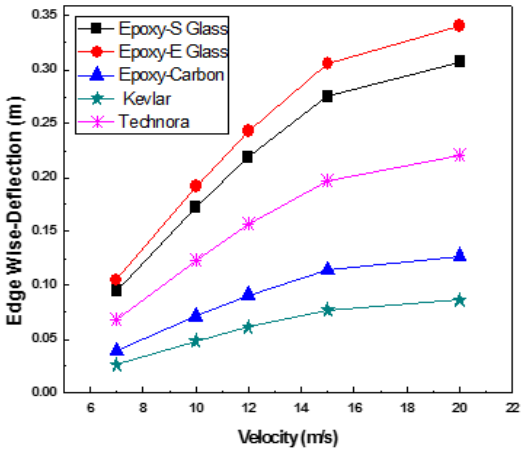

(c)

Figure 12: (a) Deformation, (b) flap-wise, and (c) edge-wise deflection for aerodynamic load only

ANSYS Result for aerodynamic load only (Deformation (m)) at V=20 m/s

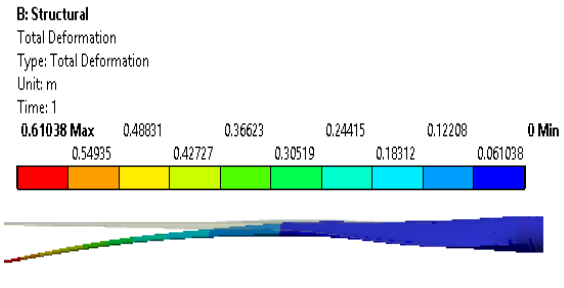

(a) Epoxy-Carbon

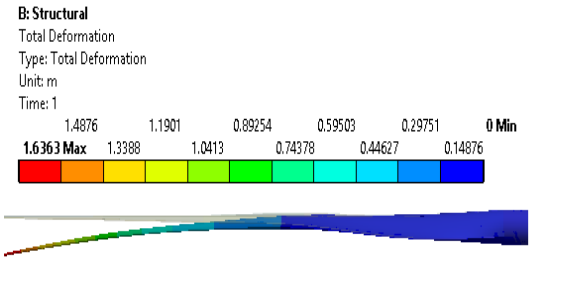

(b) Epoxy-E Glass

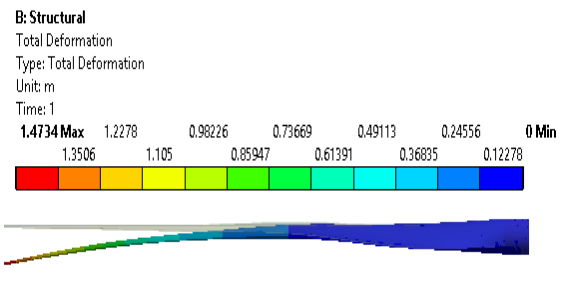

(c) Epoxy-S Glass

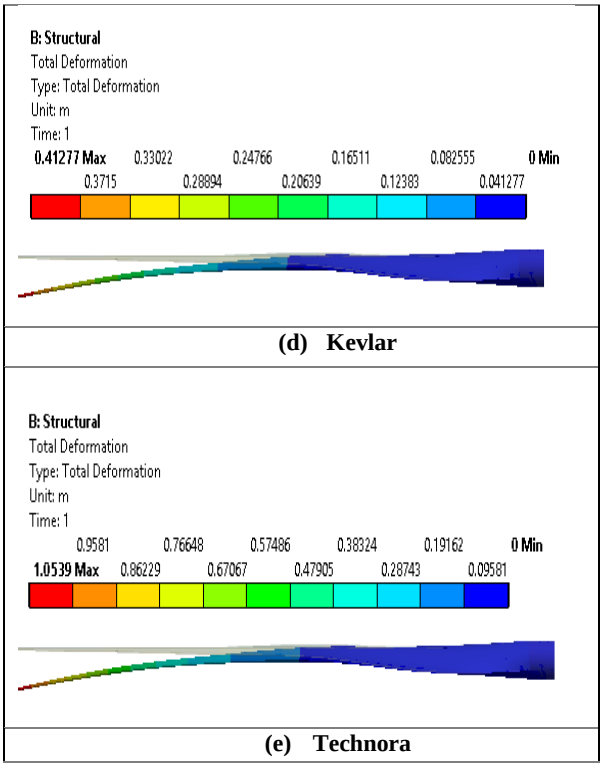

(d) Kevlar

(e) Technora

Figure 13: ANSYS Result for deflection under aerodynamic load only.

4.3. Deformation for aerodynamic, gravitational, and centrifugal loads at each blade position

Table 7 also compares the blade deformation in the case of one-way coupling after including the load combination of aerodynamic, gravitational, and centrifugal loads. Figure 14 and Figure 15 illustrate the max deformation, flap-wise, and edge-wise deflection of various composite materials under aerodynamic, gravitational, and centrifugal loads at each blade position for a velocity of 20 m/s. Under wind, gravitational, and centrifugal load operational conditions at a wind speed of 20 m/s, the maximum blade deflection of 1.4918 m is observed in the Epoxy E-Glass material at a 90-degree angle. The Kevlar material's minimum blade deflection of 0.37381 m is observed at a 270-degree angle.

The maximum blade-tip flap-wise deflection of 1.4304 m is observed in the Epoxy E-Glass material at a 90-degree angle. The minimum blade-tip flap-wise deflection of 1.4304 m is observed in the Kevlar material at a 270-degree angle. The maximum blade-tip edge-wise deflection of 0.42261 m is observed in the Epoxy E-Glass material at a 90-degree angle. The minimum blade-tip edge-wise deflection of 0.055837 m is observed in the Kevlar material at a 270-degree angle. The ANSYS results of different materials and the deformation are shown in Figure 16 and Table 6.

Table 7. Deflection for aerodynamic, gravitational, and centrifugal loads (Epoxy-Carbon)

Boundary condition		Aerodynamic, gravitational, and centrifugal Loads - (**Epoxy-Carbon**)		
Velocity (m/s)	Position	Deformation (m)	Flap-Wise Deflection (m)	Edge-wise Deflection (m)
7	**90°**	0.2681	0.2554	0.081614
	180°	0.21743	0.21377	0.039765
	270°	0.17023	0.17019	0.009532
	360°	0.2153	0.21178	0.038805
10	**90°**	0.40168	0.38585	0.11173
	180°	0.3506	0.34361	0.069726
	270°	0.30184	0.30063	0.027051
	360°	0.34971	0.34283	0.069044
12	**90°**	0.47961	0.46179	0.1296
	180°	0.42852	0.4195	0.087549
	270°	0.37978	0.37711	0.04498
	360°	0.4283	0.41938	0.087023
15	**90°**	0.57698	0.55672	0.15162
	180°	0.52277	0.51128	0.10905
	270°	0.47478	0.47008	0.066679
	360°	0.52596	0.51453	0.10909
20	**90°**	0.63928	0.61788	0.16403
	180°	0.58744	0.57469	0.12176
	270°	0.53866	0.53279	0.079287
	360°	0.58868	0.576	0.12155

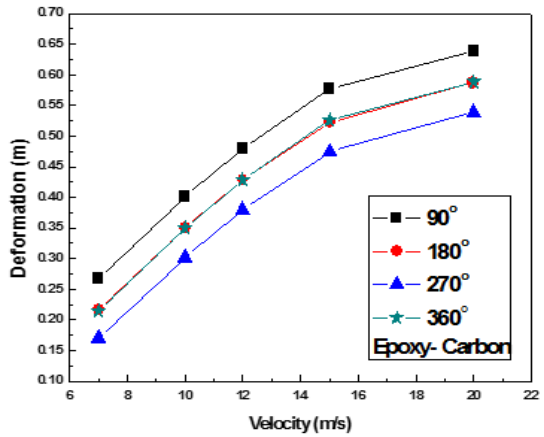

(a) Max Deformation and velocity

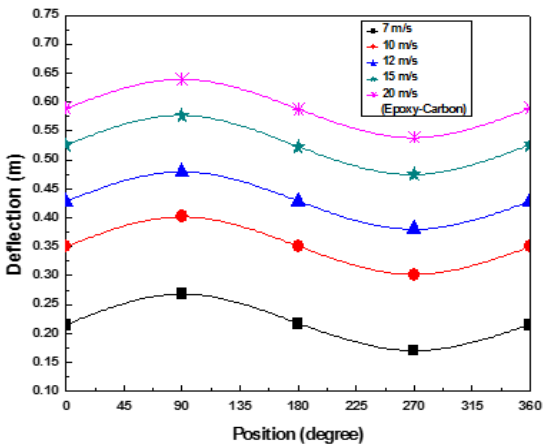

(b) Deformation and position

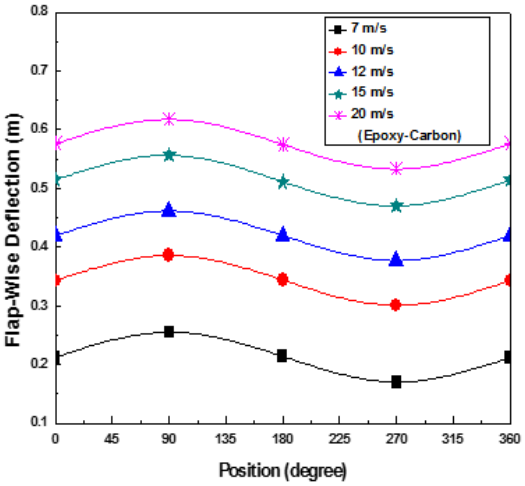

(c) Flap-wise deflection and position

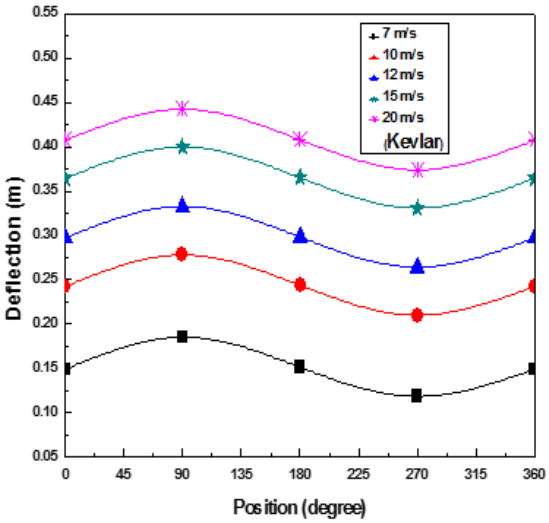

(b) Deformation and position

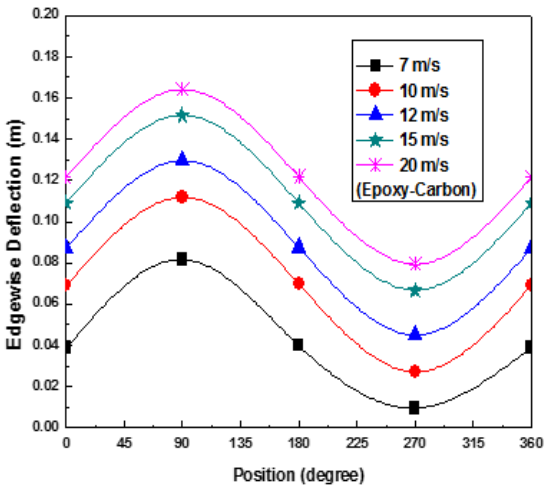

(d) Edge-wise deflection and position

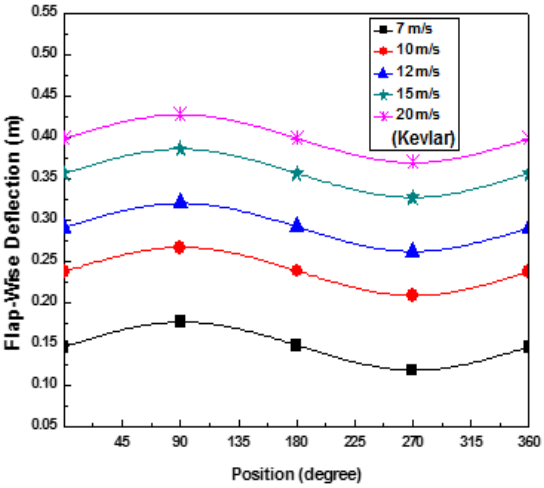

(c) Flap-wise deflection and position

Figure 14: (a-b) Deflection, (c) flap, and (d) edge-wise under aerodynamic, gravitational, and centrifugal loads operational conditions with (Epoxy- Carbon) and positions

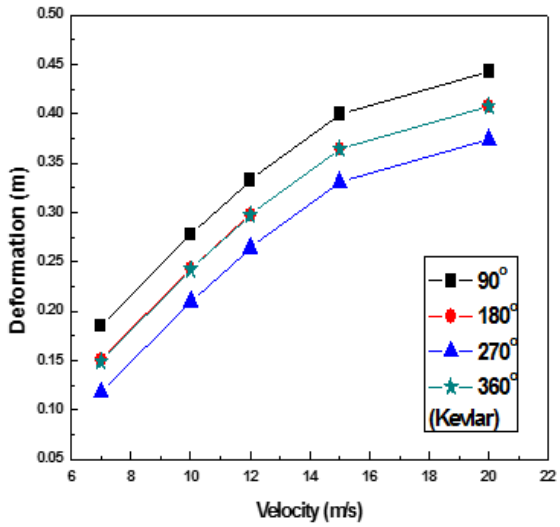

(a) Max Deformation and velocity

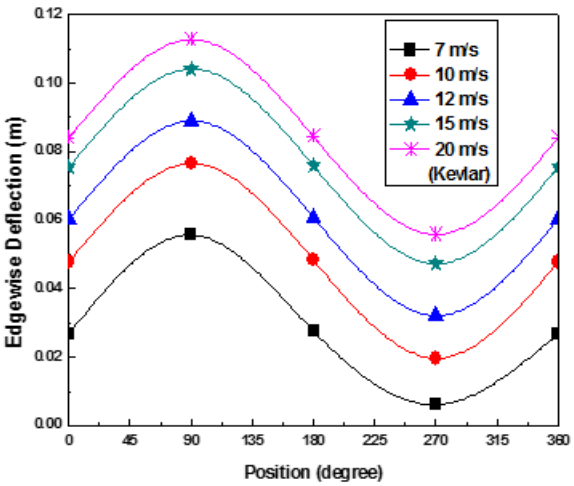

(d) Edge-wise deflection and position

Figure 15: (a-b) Deflection, (c) flap, and (d) edge-wise under aerodynamic, gravitational, and centrifugal loads operational conditions with (Kevlar) and positions

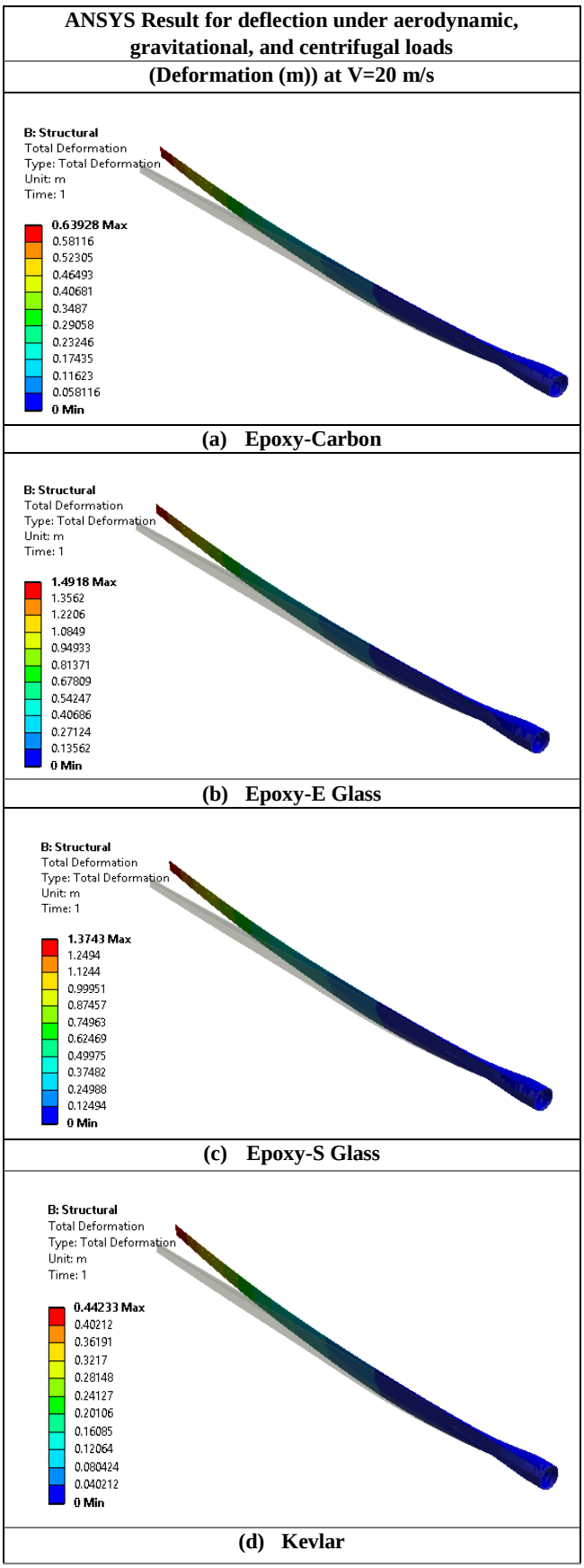

Figure 16: ANSYS Result for deflection under aerodynamic, gravitational, and centrifugal loads.

5. CONCLUSIONS

In the present study, the aerodynamic efficiency of the HAWT utilizing computational techniques in fluid dynamics has been studies. This simulation shows the workflow of creating a composite material using ANSYS and applying it for fluent and structural analysis FSI one-way. The CFD outcomes obtained have been compared to the numerical computations and experimental data of the 1.5MW turbine [16]. This study has outcomes that the CFD and FEA techniques corroborate the empirical findings and utilized to optimize the shape specifications of the turbine. The following conclusions can be drawn from the present study:

1. The blade pressure distributions are studied under five operational conditions using the FSI model. These conditions correspond to wind speeds of 7 m/s, 10 m/s, 12 m/s, 15 m/s, and 20 m/s.
2. The tip velocity value was 96.015 m/s, from analytical calculations, whereas the CFD analysis indicated a slightly higher velocity of 98.05 m/s, with a difference of approximately 2.07%.
3. The experimental power coefficient was 0.26 from the report [16], while the CFD analysis was 0.28.
4. Under wind load-only operational conditions at a wind speed of 20 m/s:
   - The Epoxy E-Glass material exhibited a maximum blade deflection of 1.6363 m, while the Kevlar material showed a minimum deflection of 0.41277 m.
   - The Epoxy E-Glass material also displayed the maximum blade-tip flap-wise deflection of 1.4405 m, whereas the Kevlar material had the minimum blade-tip flap-wise deflection of 0.40366 m.
   - Regarding blade-tip edge-wise deflection, the Epoxy E-Glass material had a maximum value of 0.30732 m, while the

Kevlar material had a minimum value of 0.086278 m.

5. Under wind, gravitational, and centrifugal load operational conditions at a wind speed of 20 m/s:
    - The Epoxy E-Glass material exhibited the maximum blade deflection of 1.4918 m at a 90-degree angle, while the Kevlar material had the minimum blade deflection of 0.37381 m at a 270-degree angle.
    - The maximum blade-tip flap-wise deflection of 1.4304 m was observed in the Epoxy E-Glass material at a 90-degree angle, whereas the Kevlar material displayed the same maximum blade-tip flap-wise deflection at a 270-degree angle.
    - The maximum blade-tip edge-wise deflection of 0.42261 m was observed in the Epoxy E-Glass material at a 90-degree angle, while the Kevlar material had the minimum blade-tip edge-wise deflection of 0.055837 m at a 270-degree angle.

These conclusions provide insights into the performance and behavior of different materials under specific operational conditions. The FSI helps optimize the design, improve efficiency, and ensure wind turbine systems' safe and reliable operation, which can be used to estimate deflection, stress, and fatigue life on the turbine blade made of composite materials.

Credit Authorship Contribution Statement

Eslam Shamso: Methodology, Software, Writing, and preparing the original draft.
Medhat El-Hadek: Reviewing and supervision.
Abla El-Megharbel: Reviewing and supervision.
Samar Elsanabary: Reviewing, editing, andsupervision.
Rasha Soliman: Reviewing, editing, and supervision.

Declaration of competing Interest

The authors declare that there is no conflict of interest regarding the publication of this paper.

Declaration of Funding

The authors did not receive support from any organization for the submitted work.

6. REFERENCES

[1] S. Mathew, Wind energy: fundamentals, resource analysis and economics, Springer, 2006.

[2] S. Jayswal, A. Bhattu, Structural and modal analysis of small wind turbine blade using three different materials, Mater. Today Proc. 72 (2023) 1347–1352. https://doi.org/10.1016/j.matpr.2022.09.329.

[3] K. Natarajan, T. Suthakar, Insight aerodynamic analysis on small-scale wind turbines airfoils for low Reynolds number applications, Environ. Prog. Sustain. Energy. 41 (2022). https://doi.org/10.1002/ep.13807.

[4] M.O.L. Hansen, Aerodynamics of Wind Turbines, 2008.

[5] P.J. Schubel, R.J. Crossley, Wind turbine blade design, Wind Turbine Technol. Princ. Des. (2014) 1–34. https://doi.org/10.1201/b16587.

[6] E.A.Z. Khazem, O.I. Abdullah, L.A. Sabri, Steady-state and vibration analysis of a WindPACT 1.5-MW turbine blade, FME Trans. 47 (2019) 195–201. https://doi.org/10.5937/fmet1901195K.

[7] R. Roul, A. Kumar, Optimized Design and Performance Testing of a 1.5 MW Wind Turbine Blade, Springer Singapore, 2021. https://doi.org/10.1007/978-981-16-0182-8_39.

[8] B.R. Resor, J. Paquette, Printed October 2012 A NuMAD Model of the Sandia TX-100 Blade, (2012).

[9] T.C.E.T. Cest, Unsteady Aerodynamics Experiment Phase VI: Wind Tunnel Test Configurations and Available Data Campaigns, (2017) 27–28.

[10] Fluent, Ansys, Ansys Fluent 16.0 Theory Guide, (2016).

[11] G. Ingram, Wind Turbine Blade Analysis using the Blade Element Momentum Method., October. 1.1 (2011) 1–21.

[12] P.J. Schubel, R.J. Crossley, Wind turbine blade design, Energies. 5 (2012) 3425–3449. https://doi.org/10.3390/en5093425.

[13] K. Lee, Z. Huque, R. Kommalapati, S.E. Han, Fluid-structure interaction analysis of NREL phase VI wind turbine: Aerodynamic force evaluation and structural analysis using FSI analysis, Renew. Energy. 113 (2017) 512–531. https://doi.org/10.1016/j.renene.2017.02.071.

[14] L. Wang, R. Quant, A. Kolios, Fluid structure interaction modelling of horizontal-axis wind turbine blades based on CFD and FEA, J. Wind Eng. Ind. Aerodyn. 158 (2016) 11–25. https://doi.org/10.1016/j.jweia.2016.09.006.

[15] R. ROUL, A. KUMAR, Effect of different pitch angles on the performance parameter of the horizontal axis wind turbine using computational fluid dynamics, Authorea Prepr. (2020).

[16] N.A. Mezaal, K. V. Osintsev, S. V. Alyukov, The computational fluid dynamics performance analysis of horizontal axis wind turbine, Int. J. Power Electron. Drive Syst. 10 (2019) 1072–1080. https://doi.org/10.11591/ijpeds.v10.i2.1072-1080.

[17] E. Shamso, M. El-Hadek, S. Elsanabary, A. El-Megharbel, R. Soliman, Finite Element Analysis for Dynamic Simulation of Composite HAWT Blade, Int. J. Renew. Energy Res. 13 (2023) 790–801. https://doi.org/https://doi.org/10.20508/ijrer.v13i2.13914.g8754.

[18] X. Cai, P. Pan, J. Zhu, R. Gu, The analysis of the aerodynamic character and structural response of large-scale wind turbine blades, Energies. 6 (2013) 3134–3148. https://doi.org/10.3390/en6073134.

[19] E. Shamso, M. Elhadek, G. Osmun, A. El-Megharbel, Fatigue Cycling of NACA 821 Blades in Horizontal Wind Turbines, SYLWAN. (2019) 79–99.

[20] M. Lipian, P. Czapski, D. Obidowski, Fluid-structure interaction numerical analysis of a small, urban wind turbine blade, Energies. 13 (2020) 1–15. https://doi.org/10.3390/en13071832.

[21] E. Shamso, A. El-Megharbel, Stress Analysis of Composite Materials in Wind Turbine Blades Subjected to CFD and FEA, SYLWAN. (2019) 330–345.

[22] Z.L. Mahri, M.S. Rouabah, Calculation of dynamic stresses using finite element method and prediction of fatigue failure for wind turbine rotor, WSEAS Trans. Appl. Theor. Mech. 3 (2008) 28–41.
[23] K. Osintsev, S. Aliukov, A. Shishkov, Improvement dependability of offshore horizontal-axis wind turbines by applying new mathematical methods for calculation the excess speed in case of wind gusts, Energies. 14 (2021). https://doi.org/10.3390/en14113085.
[24] R. Roul, A. Kumar, Fluid-structure interaction of wind turbine blade using four different materials: Numerical investigation, Symmetry (Basel). 12 (2020). https://doi.org/10.3390/sym12091467.
[25] GE General Electric GE 1.5xle - 1,50 MW - Wind turbine, (n.d.). https://en.wind-turbine-models.com/turbines/656-ge-general-electric-ge-1.5xle (accessed September 22, 2023).
[26] NREL's S818 Airfoil (s818-nr), (n.d.). http://airfoiltools.com/airfoil/details?airfoil=s818-nr (accessed September 22, 2023).
[27] T. Uchida, Y. Taniyama, Y. Fukatani, M. Nakano, Z. Bai, T. Yoshida, M. Inui, A new wind turbine CFD modeling method based on a porous disk approach for practical wind farm design, Energies. 13 (2020) 3197.
[28] G. Hren, Numerical analysis of a wind turbine blade with different software, Teh. Vjesn. 26 (2019) 1017–1022. https://doi.org/10.17559/TV-20180615151600.
[29] Y.E.S. Yassen, A.S. Abdelhameed, K.A. Elshorbagy, An examination of hub wind turbine utilizing fluid-structure interaction strategy, Alexandria Eng. J. 64 (2023) 1–11. https://doi.org/10.1016/j.aej.2022.08.042.
[30] X. Chen, Y. Liu, Finite element modeling and simulation with ANSYS workbench, 2014. https://doi.org/10.1201/b17284.
[31] S. Moaveni, Finite Element Analysis Theory and Application with ANSYS, 2007.
[32] R. Rafiee, M. Tahani, M. Moradi, Simulation of aeroelastic behavior in a composite wind turbine blade, J. Wind Eng. Ind. Aerodyn. 151 (2016) 60–69. https://doi.org/10.1016/j.jweia.2016.01.010.